Apolipoprotein A1 and high-density lipoprotein limit low-density lipoprotein transcytosis by binding scavenger receptor B1

Karen Fung[1,2], Tse Wing Winnie Ho[2,3], Zizhen Xu[4], Dante Neculai[4], Catherine A. A. Beauchemin[5,6], Warren L. Lee[1,2,3]*, Gregory D. Fairn[1,2,3,7]*

[1]Department of Biochemistry, University of Toronto, Toronto, Ontario Canada

[2]Keenan Research Centre, St. Michael's Hospital, Unity Health Toronto, Toronto, Ontario, Canada

[3]Department of Laboratory Medicine and Pathobiology, University of Toronto, Toronto, Ontario, Canada

[4]Department of Cell Biology, and Department of Pathology Sir Run Run Shaw Hospital, Zhejiang University School of Medicine, Hangzhou, China.

[5]Department of Physics, Ryerson University, Toronto, Ontario, Canada

[6]Interdisciplinary Theoretical and Mathematical Sciences (iTHEMS) program, RIKEN, Wako, Saitama, Japan

[7]Department of Pathology, Dalhousie University, Halifax, Nova Scotia, Canada.

*Correspondence should be directed to Gregory D. Fairn (gfairn@dal.ca) or Warren L. Lee (Warren.Lee@unityhealth.to)

Running title: ApoA1/HDL limit LDL transcytosis

Keywords: apolipoprotein A1, HDL, LDL, transcytosis, atherosclerosis

Abstract

Atherosclerosis results from the deposition and oxidation of low-density lipoprotein (LDL) and immune cell infiltration in the sub-arterial space leading to arterial occlusion. Numerous studies have now shown that transcytosis transports the circulating LDL across endothelial cells lining the blood vessel. LDL transcytosis is initiated by binding to either Scavenger Receptor B1 (SR-B1) or Activin A receptor-like kinase 1 (ALK1) on the apical side of endothelial cells leading to its transit to the basolateral side. Individuals with elevated levels of circulating high-density lipoprotein (HDL) are partly protected from atherosclerosis due to its ability to remove excess cholesterol and act as an antioxidant. Apolipoprotein A1 (ApoA1), an HDL constituent, can bind to SR-B1, suggesting that ApoA1/HDL may also compete with LDL for SR-B1 binding and thereby oppose its deposition in the sub-arterial space. To examine this possibility, we used in vitro approaches to quantify the internalization and transcytosis of fluorescently labelled LDL in coronary endothelial cells. Using microscale thermophoresis and affinity capture, we find that SR-B1 and ApoA1 directly interact and that binding is enhanced when using the cardioprotective variant of ApoA1 termed Milano (ApoA1-Milano). *In vivo* injection of either wild-type ApoA1 or ApoA1-Milano significantly reduced the acute accumulation of LDL in the atheroprone inner curvature of the murine aorta; inhibition was greater with Milano than the wild-type ApoA1. Together, the results suggest that an additional mechanism for HDL's atheroprotective effects is attenuating LDL transcytosis through competition for the SR-B1 receptor.

Introduction

Heart attacks and strokes arise from the development of atherosclerosis, an inflammatory disease initiated by the deposition of cholesterol-rich LDL in the intima of the arterial wall following its transit across the endothelium. This is especially apparent in regions of the vasculature that experience disturbed, non-laminar blood flow that is more prone to atherogenesis.[1] The excess intimal LDL is subject to oxidation, with the resulting oxidized LDL (oxLDL) contributing to the activation of the endothelium leading to the accumulation of monocytes/macrophages that use scavenger receptors to internalize the excess lipoproteins.[2] Unfortunately, macrophages overloaded with oxLDL cholesterol differentiate into foam cells. The accumulation of neutral

lipids in lipid droplets gives the name foam cells. However, the inability to effectively clear dead cells, egress from the subendothelial space, and death contribute to the accumulation of necrotic cells. Over time, the collection of lipids, inflammatory cells, cellular debris, and foam cells is accompanied by smooth muscle cell infiltration into the intima to form a fibrous cap overlaying the necrotic core. These lipid-laden macrophages, known as foam cells, initiate an inflammatory response in the vessel wall that leads to lesion progression, arterial luminal narrowing, and plaque rupture.

The initial step in this process is the transit of LDL across the endothelial cells' cytoplasm by the process of transcellular transport or transcytosis. In this form of transcytosis, LDL is internalized into vesicles at the apical surface and then transported through the cytoplasm and subsequently undergoes exocytosis and release at the basolateral surface. We and others have found that LDL transcytosis is mediated by its binding to the Scavenger Receptor B1 (SR-B1)[3,4] and Activin receptor-like kinase 1 (Alk1).[5] Similar to LDL, HDL must also undergo transcytosis to move from the circulation to the intima of blood vessels. This is mediated by binding to SR-B1 on the surface of endothelial cells.[6]

HDL is cardioprotective, yet the exact mechanisms by which this occurs remain unclear. The most ascribed function of HDL is as a cholesterol acceptor for reverse cholesterol transport, a process dependent on transcytosis to enter and exit the intimal space.[7] However, HDL is also an anti-inflammatory particle [8–168–10] that can promote endothelial integrity,[15,17–19 11–14]induce the production of the vasodilator prostacyclin,[20 17,1819151516]and carries miRNAs involved in vascular biology and inflammation[21] as well as SR-B1 expression.[22] We and others have demonstrated that HDL transcytosis is also mediated by SR-B1[6,23] and the ATP-binding Cassette (ABC) G1 transporters.[6] Since LDL and HDL both utilize SR-B1 to cross the endothelium, it is possible that HDL could compete with LDL for available SR-B1.

Many of the beneficial properties of HDL are attributable to its main protein component, apolipoprotein A1 (ApoA1)[24–27] found exclusively on HDL. ApoA1 is composed of several amphipathic helical motifs[28], which are required for its function to maintain the structure of the particle. Although most plasma ApoA1 exists as part of HDL, in a lipidated state, a small

transient pool of lipid-free ApoA1[29] exists to facilitate the exchange of ApoA1 amongst different populations of HDL. Referred to as HDL-ApoA1 Exchange (HAE), this process is reduced in patients with atherosclerosis or those carrying at least one risk factor of CVD.[30] Importantly, hypoalphalipoproteinemia, a disorder where ApoA1 mutations prevent its synthesis, led to lowered plasma HDL levels and premature cardiovascular diseases.[31,32] Together, this highlights the importance of ApoA1 in lipid-free and lipid-associated forms in providing protective effects impeding cardiovascular pathogenesis. Furthermore, naturally occurring ApoA1 variants have been identified to have variable phenotypes. In particular, ApoA1-Milano is a variant with a mutation at arginine 173 for cysteine that facilitates the formation of an intermolecular disulphide bond between two ApoA1 molecules.[33] Curiously, carriers of the ApoA1 Milano mutation have lower plasma HDL and ApoA1 levels (by about 50%), elevated triglycerides, shift in HDL subtypes with elevated HDL_3 and decreased HDL_2,[34,35] but exhibit a low incidence of CVD.[33,36]

Given that both HDL and LDL can bind to SR-BI, we hypothesized that competition for the receptor (and thus inhibition of LDL transcytosis) could be another mechanism by which HDL protects against atherosclerosis. We now provide evidence that recombinant ApoA1 antagonizes LDL internalization and transcytosis in HCAECs. This was potentiated when ApoA1 was reconstituted as minimally lipidated HDL. The data also suggest ApoA1-Milano is a better ligand for SR-B1 than the wild-type protein. Together, the results reveal an unappreciated mechanism by which ApoA1/HDL is anti-atherogenic.

Methods

Cell Culture

Human coronary artery endothelial cells (HCAECs, Promocell – C-12221, lot 425Z019.1) were cultured in EGM2TM BulletKit™medium (Lonza Switzerland, CC-3162) and grown at 37˚C at 5% CO_2. Henrietta Lack cells (HeLa, ATCC) were cultured in Dulbecco's Modified Eagle's Medium (DMEM, Corning) supplemented with 10% FBS (Wisent) and grown in the same environmental conditions. For the HCAECs, the medium was changed every 2 to 3 days of culture and experiments were performed at least 2 days after seeding on 0.1% gelatin-coated 25 mm round coverslips.

DNA Transfection

HeLa cells were transfected using X-tremeGENE™ HP DNA transfection reagent (Sigma-Aldrich) at a ratio of 1:3 using 0.5 μg of DNA in 100 μL of Opti-MEM per 12 well. Cells were transfected 1 day after seeding, and internalization experiments were performed 1 day after transfection.

Production of ApoA1 Mutants

ApoA1 variants were generated using the Phusion Site-Directed mutagenesis Kit (Thermo Fisher Scientific), E.coli codon-optimized cDNA encoding human ApoA1[23] and the following primers:
Milano:
Forward: AACTGCGGCAATGCCTTGCAGC
Reverse: CGTCAGAGTACGGCGCGAGATGTG
Expression and Purification of the ApoA1 variants were performed using ClearColi® BL21(DE3) (Lucigen).[23] ApoA1 was eluted from Talon® Metal Affinity Resin (Takara) using 0.1 M EDTA. Eluants were dialyzed with PBS at 4˚C to remove 0.1 M EDTA and any residual Guanidine HCl; the dialysis buffer was changed twice before ApoA1 protein collection. Purity was assessed by running dialyzed eluants on SDS-PAGE, and concentrations were calculated using the molar extinction coefficient of ApoA1 at 280 nm and measuring the absorbance at 280 nm.

Cloning and purification for microscale thermophoresis experiments

The full-length ApoA1-WT, ApoA1-Milano, and the N-terminal His_6-tagged luminal domain of human SR-B1 (amino acid 33 – 444) were cloned into PB-T-PAF[37] downstream and in frame with the protein A tag (protein A-ApoA1, protein A-ApoA1-Milano, and protein A-His_6-*h*SR-B1[38]), by using a two-step PCR strategy with overlapping primers encompassing the desired mutation and sequence verified.

Recombinant ApoA1, ApoA1-Milano, and His-tagged SR-B1 ectodomain (His_6.*h*SR-B1 (amino acid 33 - 444)) were expressed in 293F mammalian cells[37] and purified as described previously.[38] The protein concentrations were quantified by BCA Protein Quantification.

Generating reconstituted HDL particles containing ApoA1 Variants

Incorporation of ApoA1 to DMPC and DiI

Lipid-associated ApoA1 were generated following previous protocols with slight modifications.[39,40] Briefly, 1,2-dimyristoyl-sn-glycero-3-phosphocholine (DMPC) (Avanti Polar Lipids), with or without 1,1' -Dioctadecyl-3,3,3',3'-Tetramethylindocarbocyanine Perchlorate (DiI) (Sigma), were transferred to a 5 mL or 10 mL round bottom flasks manufactured from borosilicate 3.3 glass with a 14/20 Joint size (VWR) and dried to a film by streaming N_2. This film was resuspended in methanol and dried to film by N_2 streaming. The film was resuspended in 25 mM HEPES in PBS and sonicated at 24˚C for 20 min or until the lipid film was fully resuspended. Recombinant ApoA1 equilibrated to 24˚C was added to the resuspended lipids, and further sonicated for 30 min at 24˚C or until turbidity disappeared. This solution was incubated at 24˚C overnight to allow ApoA1 incorporation into vesicles.

Potassium Bromide Gradient Ultracentrifuge

Lipidated ApoA1 was separated by buoyancy in a KBr gradient by ultracentrifugation. Briefly, the lipidated ApoA1 was transferred to the bottom of a ½-inch × 2-inch ultracentrifuge tube and topped to 2 mL using PBS containing 0.3 mM EDTA. The density of this solution was adjusted to [2.45-2.5] g/mL using KBr. An additional 2 mL of 1.063 g/mL PBS containing 0.3 mM EDTA was layered on top. This was then subjected to centrifugation at 35,000 rpm for 24 h at 4˚C in a Beckman Optima LE-80 Ultracentrifuge using a SW55Ti rotor with maximum acceleration and without breaking at the end of the spin. Next, 200 μL fractions were collected, and density was calculated by measuring the weight of the 200 μL fraction. Absorbances at 280 nm and 555 nm were measured using the NanoDrop™ 2000/2000c (Thermo Scientific) to determine the presence of ApoA1 and DiI (respectively) in each fraction. Fractions corresponding to the appropriate densities containing sufficient ApoA1 were pooled and dialyzed to remove the dialysis.

Native Gel Electrophoresis of Lipoproteins

Samples were resolved using a 4-12% polyacrylamide gradient gel (pH 8.75) using the Tris-glycine buffer system. The gel was first imaged to detect the DiI label and then stained with Coomassie to detect protein.

Internalization Experiments

DiI-LDL Internalization

HCAECs were washed twice with cold Dulbecco's Phosphate Buffered Saline supplemented with calcium and magnesium (PBS+, Sigma). 10 μg/mL DiI-LDL in the presence of PBS or the various unlabelled ApoA1 variant or $rHDL^{ApoA1}$ (of density 1.1 g/mL) in serum-free RPMI (Gibco, 1640) were incubated with HCAECs for 20 min at 37˚C to allow for internalization. After 20 min, DiI-LDL was removed, and HCAECs were washed twice with PBS+ and fixed in 4% paraformaldehyde.

DiI-$rHDL^{ApoA1}$ Internalization

HeLas were washed twice with PBS+, and 5 μg/mL of DiI-labelled rHDL with different ApoA1 variants (DiI-$rHDL^{ApoA1}$) in the presence of PBS or the various unlabelled ApoA1 variant proteins in DMEM supplemented with 5% BSA were incubated with HeLa cells for 1 h at 37˚C to allow for internalization. After 1 h, the DiI-$rHDL^{ApoA1}$ was removed, and HeLa cells were washed twice with PBS+ and fixed in 4% paraformaldehyde.

Microscopy

The Quorum (Guelph, Ontario) Diskcovery spinning disk confocal/TIRF system was used to image the DiI-LDL. This system is based on a Leica DMi8 with a Nipkow spinning disk with a pinhole size of 50 μm, a Hamamatsu ImageEMX2 EM-CCD camera, with diode-pumped solid-state lasers (405 nm, 488 nm, 561 nm and 637 nm) and a 63x oil immersion objective with a 1.47 numerical aperture. For DiI-$rHDL^{ApoA1}$ internalization, a Quorum spinning disk confocal microscope (Yokogawa CSU-X1 spinning disk head with Borealis, Hamamatsu ImageEMX2 EM-CCD camera at 63x objective, numerical aperture 1.4, with diode-pumped solid-state lasers 405 nm, 488 nm, 552 nm and 730 nm) was used. In both experiments, z-slices encompassing the whole cell were acquired at intervals of 0.2 μm.

Analysis and Quantification

The amount of DiI-LDL and DiI-$rHDL^{ApoA1}$ internalization per cell was calculated by the sum of the raw integrated density of the DiI channel within the region of interest (the cell) across all z-slices measured using Fiji (NIH). Due to the varying sizes of HeLa cells in the DiI-$rHDL^{ApoA1}$ experiments, which may affect the absolute total DiI-$rHDL^{ApoA1}$ fluorescence, the summed raw

integrated density of DiI-ApoA1 was further normalized by dividing by the volume of the cell which was calculated by multiplying the area of the cell (the region of interest from which the raw integrated density was measured from as determined by the GFP channel) by the number of slices analyzed. Values plotted for DiI-LDL internalization are the absolute DiI-LDL fluorescence per cell analyzed. Values plotted for DiI-rHDL^{ApoA1} internalization are normalized to the DiI-rHDL^{ApoA1} uptake seen in the GFP transfected alone control.

In vitro ApoA1-SR-B1 Binding Assay

The interaction between SR-B1 and ApoA1 or rHDL was assessed through an *in vitro* binding assay using GFP nanotrap beads. The GFP nanotrap was made as previously.[41] For the binding assay, HeLa cells overexpressing GFP-SR-B1 or GFP alone (control) were lysed in lysis buffer (0.5% NP-40, 10 mM glycine, protease inhibitor in PBS). The soluble fraction of the lysates (supernatant after centrifugation for 13,000 rpm for 10 min at 4°C) were incubated with pre-equilibrated GFP nanotrap beads overnight with end-to-end rotation at 4°C to immobilize GFP or GFP-SR-B1 onto beads. The beads were washed 3x with lysis buffer, after which the ApoA1 variant protein was added and topped with PBS to a final total volume of 1 mL. This reaction was further incubated with end-to-end rotation at 4°C for 3 h to allow for the ApoA1 interaction with GFP or GFP-SR-B1. The GFP or GFP-SR-B1 beads were then washed 3x - 4x with high salt (1.5 M) PBS to remove non-specific interaction, and SDS-PAGE loading buffer (either in the presence or absence of DTT, where indicated) was added to elute remaining proteins off the beads. The sample was analyzed through western blot and immunoblot with antibodies against ApoA1 (Abcam, clone [EP1368Y]) and GFP (Bio X Cell, clone [F56-6A1.2.3]) to assess the amount of rHDL^{ApoA1}or ApoA1 bound and the amount of GFP or GFP-SR-B1 immobilized between different conditions.

Microscale thermophoresis (MST)

MST experiments were performed on a Monolith NT.115 instrument (NanoTemper Technologies). Purified His-tagged SR-B1 protein (His$_6$.*h*SR-B1(amino acids 33 - 444), was labelled using the Monolith His-Tag Labeling Kit Red-tris-NTA (NanoTemper Technologies) and diluted in MST buffer (NanoTemper Technologies) to a concentration of 50 nM, was mixed with ApoA1 or ApoA1-Milano in MST buffer (PBS with 0.05%Tween) at indicated concentrations ranging from 1 nM to 8 μM at room temperature. Fluorescence was determined in

a thermal gradient at 40% LED power and high MST power generated by a Monolith NT.115 from NanoTemper Technologies. Data were analyzed using Affinity Analysis v2.3.

Measuring Transcytosis Using Total Internal Reflection Fluorescence Microscopy

Transcytosis Assay

Total internal reflection fluorescence (TIRF) microscopy was conducted using live HCAEC monolayers seeded on glass coverslips and placed in a chamblide imaging chamber. Videos were taken using the Quorum Diskcovery TIRF system, where 150 images were taken at 100 ms exposure with a penetration depth of the illumination of 100 nm into the basal membrane.

Confluent monolayers were pre-chilled for 5 min in cold HEPES-buffered RMPI (HPMI) media at 4˚C. HPMI media was removed, and 20 µg/mL DiI-LDL with the recombinant ApoA1 variant or $rHDL^{ApoA1}$ or PBS in cold HPMI was added and incubated for 10 min at 4˚C to allow binding. Cells were then washed twice with cold PBS+ to remove unbound ligand, and prewarmed HMPI was added, after which the cells were placed on the live imaging stage. After approximately 1 min 45 s, imaging of the cell began. Cells in confluent regions, identified through the number of nuclei in the DAPI channel stained by Nucblue™ Live cell staining (Thermo Fisher Scientific) added at the membrane-binding step, were imaged. A total of 10 fields of view were imaged per condition, where videos acquired were staggered by about 1 min.

Post-Acquisition Analysis

The number of exocytosis events was calculated using a previously developed single-particle-tracking algorithm[3,42] with modifications.[43] Briefly, the local background signal was subtracted, and images were thresholded to create a binary image (mask). Putative vesicles were identified based on size (60 nm to 200 nm in diameter), circularity (>0.2), and intensity (threshold of 15% above mean image intensity). Vesicles were tracked based on maximum probability, which was dependent on the change in centroid particle and change in peak intensity. Exocytosis involves vesicles docking at the PM before membrane fusion and cargo release; hence the identification of transcytosis events was limited to vesicles that were stationary (potentially docked). Vesicle diffusivity (mean-squared displacement) was quantified, and those exhibiting subdiffusive behaviour before exocytosis ($\alpha<1$) were included. From this subdiffusive population, vesicles

that underwent a reduction of at least 3 standard deviations in fluorescent intensity during the last 5 time points of their tracks and did not reappear for 5 subsequent frames were counted as exocytosis events.

LDL Perfusion of Mouse Aorta

The acute accumulation of LDL in the inner curvature of the murine aorta was measured as previously reported.[44] Briefly, male C57BL/6J mice (Jackson Laboratory) were housed in a temperature-controlled room on a standard 12 h light-dark cycle, with *ad libitum* access to water and food. All experiments were conducted during the light phase of the cycle, between 10 weeks to 13 weeks of age. All experimental procedures were approved by St. Michael's Hospital Animal Care Committee (ACC 899) and were in accordance with the guidelines established by the Canadian Council on Animal Care. Mice were anesthetized and administered vehicle (PBS+), 0.4 mg ApoA1 WT, or 0.4 mg ApoA1 Mil by retro-orbital injection. Thirty minutes later, mice were administered 200 µg of Alexa Fluor 568 conjugated-LDL via retro-orbital injection. After 30 min, mice were euthanized by exsanguination and aortas were slowly perfused with 5 ml of PBS containing calcium and magnesium followed by 5 ml of 10% buffered formalin through the left ventricle. Hearts were then dissected and fixed with 10% buffered formalin for 60 min. After fixation, adventitial fat and tissue on the aortic arch were removed using microdissection scissors. The aortic arch was removed from the descending aorta, aortic branches, and aortic root.

Aortas were permeabilized with 0.5 % Triton X-100 and 10 % DMSO in PBS+ for 5 min. After washing, aortas were incubated with 10 µg/ml rabbit anti-mouse CD31 primary antibody (NB100-2284; Novus) in 5% BSA at 4ºC overnight. Aortas were then washed and incubated with 7.5 µg/ml anti-rabbit Alexa Fluor 488 secondary antibody (Jackson ImmunoResearch) in 5 % BSA at room temperature for 1 h, followed by 2.5 ug/ml DAPI (Roche) for 20 min. After washing, aortas were mounted *en face* with Dako fluorescence mounting medium (Agilent).

The entire aortic arch was imaged using a ZEISS LSM 700 microscope with 20x/0.8 objectives: 405 nm, 488 nm, 555 nm, and 639 nm laser lines with settings kept constant between conditions. All acquisitions were acquired with ZEN Black software. ImageJ was used to subtract

background fluorescent signal to quantify LDL deposition, and integrated densities of Alexa Fluor 568-LDL were quantified and normalized to the aortic (CD31 positive) area.

Statistics and Graphic Representation

Each experiment was repeated n times, and within each experiment (each k out of n), where each n represents an experiment done at a different time and using a different passage of cells. The fluorescence of several individual cells was measured either with cells alone (**blank**) or in the presence of a fluorescently tagged compound (e.g. DiI-LDL) to which either **control** is added (e.g. PBS) or a **condition** is investigated (e.g. addition of an ApoA1 variant).

For LDL transcytosis experiments using recombinant ApoA1 as competitors, LDL internalization experiments using $rHDL^{ApoA1}$ as competitors, $rHDL^{ApoA1}$internalization experiments using recombinant ApoA1 as competitors, and the internalization of DiI-DMPC particles that lack ApoA1 experiments, the graphs were generated using GraphPad Prism 5.0 (GraphPad Software Inc., La Jolla, CA, USA), where data were presented as averages per experiment ± SEM. The statistics were performed using Student's t-test or ANOVA (GraphPad Prism 5.0; GraphPad Software Inc., La Jolla, CA, USA) with Bonferroni's or Dunn's selected *Post-hoc* for raw or normalized data (respectively).

For the LDL internalization experiments and LDL transcytosis experiments using $rHDL^{ApoA1}$ as competitors, the graphs were generated using python's matplotlib library. The change in fluorescence for a given condition, relative to the control (ctrl), for experiment replicates k, was computed as:

Change_ctrl_k = { [ctrl_i – mean(blank)] / [ctrl_j – mean(blank)] } for all i,j
Change_cond_k = { [cond_i – mean(blank)] / [ctrl_j – mean(blank)] } for all i,j

Where: cond_i is the fluorescence for each cell under the condition (i.e. I from 1 to Ncells_cond), ctrl_j is the fluorescence for each cell in control (i.e. j from 1 to Ncells_ctrl), and mean(blank) is the average fluorescence for all cells alone.

As such, Change_cond_k is a set of fluorescence measures for experiment replicate k, represented as dots of the same colours in such figures, and there are Nchange_k = Ncells_cond * Ncells_ctrl, such measures in each replicate k of the n total, replicates conducted for each control or condition. Because steps in Change_cond_k are relative to both blank and control measurements, the conditions within a particular experiment are thus subtracted so the set of n replicates of Change_cond_k sets can be combined as a single set, Change_cond, which contains Nall = Nchange_k * n points. The bars appearing next to the dots correspond to the edge of the 95th (dark grey) and 68th (light grey) percentiles and the median (black horizontal bar) for the Change_cond set of measurements.

The fold-change and p-value between the control and the condition are computed by taking each of the Nall_cond points in Change_cond and dividing them by each of the Nall_ctrl points in Change_ctrl. The median and 95th percentile of this set of Nall_cond * Nall_ctrl points are reported in the text. If the condition corresponds to an increase in fluorescence, i.e. if the median fold-change is greater than one, the p-value is the probability of the null hypothesis, i.e. that the condition does not correspond to an increase in fluorescence (fold-change equal to or less than one). This is computed as the Binomial likelihood of get f_fail times n_trial failures out of n_trial attempts. Here f_fail is the fraction of the Nall_cond times Nall_ctrl points where the fold-change was equal to or less than one, and n_trial is the number of independent points which is not Nall_cond * Nall_ctrl. Indeed, while set Change_ctrl contains Ncells_cond times Ncells_ctrl measures, these measures are not completely independent in that each cond_j is re-used Ncells_ctrl times, i.e. divided by all ctrl_j measures. To correct for this, we take n_trial as the sum of the number of cells whose fluorescence was measured under the condition for each replicate, i.e. n_trial is the sum of Ncells_cond for each of the n replicates.

For the other experiments, a student's t-test was utilized. For LDL perfusion in vivo experiments, 1-way ANOVA was performed using GraphPad Prism software, version 9.0 (La Jolla, CA, USA). Individual comparisons between samples were analyzed using Šidák post hoc test and data were presented as mean per experiment ± SEM.

Results

Inhibition of LDL Transit Across the Endothelium by Excess Recombinant Wild-Type ApoA1

To address whether wild-type ApoA1 (ApoA1-WT) can inhibit LDL transit across endothelial cells, recombinant ApoA1 was expressed and purified from ClearColi™, an E.coli mutant deficient in lipopolysaccharide (**Supplemental Figure 1**).[23] First examined the effect of unlabelled ApoA1on DiI-LDL internalization in human coronary artery endothelial cells (HCAECs). After incubation of DiI-LDL and unlabelled ApoA1 with HCAEC for 15-20 min at 37˚C, cells were washed, fixed, imaged using confocal microscopy and subsequently analyzed using ImageJ to measure the amount of LDL internalization by quantifying the fluorescence intensity of DiI. The internalization of DiI-LDL by the primary HCAECs (**Supplemental Figure 2A**) exhibited high variability, likely due to passaging the primary human cells as such cells displayed 10^4 to 10^6 fluorescence units (total integrated fluorescence per cell) (**Supplemental Figure 2B**). This variability made the assay less sensitive in detecting subtle changes in DiI-LDL internalization. Hence the DiI-LDL fluorescence signal of each cell per condition was compared to each cell in control (PBS alone), and the median change was compared between treatments. As a result, a 20-fold excess of unlabelled ApoA1 led to a significant (p-value = 10^{-6}) 1.96-fold reduction (median fold change of 0.51 or log2(-0.97)) [95% CI: (0.035, 150.4)] in the median DiI-LDL internalization compared to the PBS treated control cells (**Figure 1B)**. This suggests that ApoA1 inhibits the internalization of DiI-LDL in HCAECs.

To determine whether the inhibition of LDL internalization impacts transcytosis, we monitored the appearance of DiI-LDL in the TIRF plane of confluent monolayers. The presence of a 20-fold excess of unlabelled ApoA1-WT with DiI-LDL during the receptor-binding step performed in the cold with HCAECs led to a significant decrease in DiI-LDL transcytosis by approximately 40% compared to DiI-LDL alone (PBS control) (p-value < 0.05) (**Figure 1C**). Together these results demonstrate that ApoA1 can cause a partial reduction of LDL internalization and that the attenuated uptake correlates with less release of LDL by transcytosis.

Reconstituted HDL is a Better Competitive Inhibitor than Free-ApoA1

Given that lipid-free recombinant ApoA1 shows a weaker SR-B1 association[40] we generated reconstituted ApoA1 ($rHDL^{ApoA1}$) and examined its ability to inhibit LDL uptake and transcytosis. ApoA1-WT was incorporated into unlabelled HDL-like particles consisting of 1,2-dimyristoyl-sn-glycero-3-phosphocholine (DMPC). Characterization of particle size and density of the resulting ApoA1-WT particles ($rHDL^{WT}$) indicated similar properties with native human HDL (**Supplemental Figure 3**). Due to the preferred association of SR-B1 with HDL_2 compared to HDL_3,[45] $rHDL^{ApoA1}$with densities similar to that of HDL_2 were used in subsequent experiments.

The ability of $rHDL^{WT}$ to inhibit LDL internalization was examined in a dose-dependent manner. Various concentrations of $rHDL^{WT}$ (10-, 5-, 1- fold excess relative to LDL by protein mass) were tested, noting that a 1-to 2-fold excess represents the physiological ratio of HDL to LDL in healthy individuals. As expected, a dose-dependence was observed where the concentration of $rHDL^{WT}$ correlated with the percent inhibition of LDL internalization. Treatment with 10-fold excess $rHDL^{WT}$ reduced the LDL internalization by ~72% (p-value <0.0001), whereas about a 50% decrease was seen at 5-fold excess $rHDL^{WT}$ (p-value = 0.001) followed by a 25% decrease with 1-fold excess (p-value = 0.008) (**Figures 1D, E**). This suggests that at physiologically relevant concentrations, 1- to 2-fold excess of $rHDL^{WT}$, HDL trends towards partial inhibition of LDL internalization by HCAECs. Given the interest in SR-B1-mediated transcytosis, $rHDL^{WT}$ was tested for its ability to inhibit DiI-LDL transcytosis using TIRF microscopy. In this assay, co-incubation of the various doses of $rHDL^{WT}$ partially inhibited DiI-LDL transcytosis (1x = 20.7%, p-value = 0.001; 2x = 18.5%, p-value = 0.003; 5x = 19.2%, p-value = 0.003). Together, these results demonstrate that for physiological ratios of HDL to LDL, LDL uptake and transcytosis are attenuated (**Figure 1F**).

ApoA1-Milano is a better SR-B1 ligand than ApoA1-WT.

ApoA1-Milano patients are protected from atherosclerosis, yet the mechanism for this protection is unknown. We hypothesized that since ApoA1-Milano can form a homodimer and SR-B1 can multimerize,[46] perhaps an increase in avidity makes ApoA1-Milano, and the resulting HDL,

better ligands for SR-B1. If so, this raises the possibility that ApoA1-Milano / HDL is a better inhibitor of LDL transcytosis. Indeed, the low circulating HDL levels in ApoA1-Milano patients could result from enhanced transcytosis of Milano HDL out of the bloodstream. To examine this possibility, we generated fluorescently labelled $rHDL^{WT}$ and $rHDL^{Mil}$ (DiI-$rHDL^{WT}$and DiI-$rHDL^{Mil}$, respectively) by including DiI during the process of particle formation. Next, we used these particles to monitor SR-B1 mediated internalization by confocal microscopy. HeLa cells transfected with a bicistronic vector encoding unlabelled SR-B1 and a soluble GFP (**Supplemental Figure 4A, B**) were used to measure the uptake of DiI-HDL. Compared to HeLa cells expressing soluble GFP or those expressing GFP-Alk1, the SR-B1 expressing cells displayed an almost 10-fold increase in fluorescence when incubated with DiI-$rHDL^{wt}$ and close to 15-fold for DiI-$rHDL^{Mil}$ (**Figure 2A, B**). As a control, DiI containing DMPC liposomes (DiI-DMPC) devoid of ApoA1 showed minimal uptake by SR-B1 expressing Hela cells (**Supplemental Figure 4C**).

Next, we sought to more directly examine the ability of ApoA1 to interact with SR-B1. To test this possibility experimentally, we first performed an *in vitro* binding assay by immobilizing SR-B1-GFP overexpressed in HeLa cells onto GFP binding nanotrap beads, followed by incubation with recombinant ApoA1-WT or ApoA1-Milano. Association with SR-B1 was assessed by immunoblotting with α-ApoA1 to detect the amount of ApoA1 protein that remains immobilized in the beads (interacting with GFP-SRB1). As shown in **Figure 2C, D**, ApoA1-WT binding to SR-B1-GFP was detected on the western blot through the presence of the ApoA1 band around 25 kDa. In parallel, the binding of ApoA1-Milano to the immobilized SR-B1 was also analyzed. As shown in **Figure 2C, D**, 2-3-fold more ApoA1-Milano was captured with SR-B1-GFP when normalized to input. As a control, ApoA1-WT and ApoA1-Milano were also incubated with GFP alone immobilized onto the GFP binding nanotrap beads, which resulted in no ApoA1 bands indicating the specificity of binding.

Complementary to the *in vitro* binding assay, we determined the binding affinities of the ApoA1-WT and Milano to the ectodomain domain of SR-B1. Using microscale thermophoresis,[47] we detected a direct interaction between the recombinant His tagged SR-B1 ectodomain (His_6.*h*SR-B^{33-444}) protein and full-length ApoA1 and ApoA1-Milano and determined the apparent Kd

values to be 6.87 μM ± 0.23 μM for ApoA1-WT and 2.06 μM ± 0.46 μM for ApoA1-Milano, respectively (Fig 2E).

Recombinant ApoA1-Milano inhibits LDL internalization and transcytosis.

Since ApoA1-WT inhibits the uptake and transcytosis of LDL (Figure 1), we next examined if this ability is also present in the ApoA1-Milano. First, DiI-LDL endocytosis was monitored in the HCAECs incubated with ApoA1-WT or ApoA1-Milano and compared to control cells treated with PBS. As shown in **Figure 3A, B**, the addition of 20-fold excess of both ApoA1 molecules decreased uptake. Specifically, the presence of 20-fold excess of unlabelled recombinant ApoA1-Milano also led to a significant (p-value = 10^{-12}) 2.9-fold median reduction (median fold change of 0.347 or log2(-1.53)) [95% CI (0.05, 326.8)] in DiI-LDL fluorescence compared to DiI-LDL alone (PBS), indicative of a decrease in DiI-LDL internalization in HCAECs. Compared to ApoA1-WT, ApoA1-Milano appeared to be a slightly better inhibitor of LDL internalization (p-value < 0.05). Additionally, we find that ApoA1-Milano can attenuate LDL transcytosis by ~40%, comparable to ApoA1-WT (**Figure 3C**). Together these results suggest that the Milano mutation and the homodimerization of ApoA1 do not impact the ability of ApoA1 to compete for LDL internalization.

As previously noted, ApoA1, when present in HDL particles, is a better ligand for SR-B1 than as a free protein. Thus, we generated rHDL containing ApoA1-Milano and assessed its ability to block LDL internalization and transcytosis by HCAECs ranging from physiological concentrations to supraphysiological levels up to 10-fold higher. As displayed in **Figure 4A** and quantified in **Figure 4B**, a physiological (1x) amount of $rHDL^{Mil}$ reduced LDL uptake by ~40% (p-value = 0.02), while 5x in $rHDL^{Mil}$ led to inhibition of LDL uptake by ~50% (p-value = 0.0002) and 10x showed inhibition of ~60% (p-value = 0.0006). This degree of inhibition is comparable to genetically silencing SR-B1. This suggests that under physiological conditions, $rHDL^{Mil}$ inhibits most of the LDL internalization dependent on the SR-B1 receptor but has minimal impact on the ALK1 mediated internalization. Furthermore, the degree of inhibition caused by the $rHDL^{Mil}$ at physiological concentrations was comparable with a slight tendency towards being greater than that obtained with the wild-type containing rHDL (**Figure 1D)**. Additionally, the impaired internalization of DiI-LDL translates to a ~22.6% decrease in LDL

transcytosis at physiological conditions (or 1x excess, p-value = 0.001) with minimal impact of the supraphysiological amounts of HDL^{Mil} (2x = 11.5% decrease, p-value = 0.04; 5x = 21.1% decrease, p-value = 0.003) (**Figure 4C**). Together these results demonstrate that Milano containing HDL is an inhibitor of LDL uptake and transcytosis.

The effects of ApoA1 Milano on LDL deposition *In vivo*

Thus far, the results suggest that ApoA1-Milano may be a better competitor than ApoA1-WT in blocking LDL uptake but may not translate to the number of exocytic events measured in our TIRF assay. Furthermore, the implications of our biochemical and cell-based studies suggest that ApoA1/HDL and the Milano variant may influence atherosclerosis development by limiting LDL deposition in arterial walls. Such a finding is important to the field; thus, we wanted to examine the possibility in a mouse model. This serves two purposes; in addition to measuring the biological significance of ApoA1 in preventing LDL accumulation, this *in vivo* approach has a longer end timepoint compared to the *in vitro* experiments. Hence differences in phenotype may be easier to detect/measure. Unfortunately, due to the scale required and the setup of the *in vivo* experiment, we could not generate a high enough concentration of rHDL for this assay, so instead, we used the free protein. To this end, the ApoA1 variants were tested to block the deposition of injected fluorescently labelled LDL (AF-LDL) in the aorta in C57BL/6J, 10 to 13-weeks-old male mice (**Figure 5A**). As shown in **Figure 5B**, retro-orbital injection of AF568-LDL led to its deposition in the inner curvature of the aorta within 30 min. LDL deposition was impeded by approximately 30% (p-value <0.05) when 2-fold excess (by mass) of wildtype ApoA1 protein was perfused before the fluorescently labelled LDL. Strikingly, perfusion of ApoA1-Milano before AF568-LDL was able to block LDL deposition by about 60% (p-value < 0.0001), indicating that ApoA1-Milano is a superior inhibitor of LDL transcytosis compared to its wildtype counterpart.

Discussion

HDL is cardioprotective through several potential mechanisms. HDL is well known to accept cholesterol for reverse cholesterol transport. However, HDL is also an anti-inflammatory particle[8–10] and is known to carry proteins such as ApoA1, Paraoxonase 1 (Pon1) and platelet-

activating factor acetyl hydrolase (PAF-AH) that are anti-oxidative proteins.[11–14] HDL has been shown to induce the production of the vasodilator prostacyclin,[20] promotes endothelial integrity by inhibiting oxidized LDL-induced apoptosis[17,18] and through SR-B1, stimulates endothelial cell migration for wound healing[19] and nitric oxide production.[15] Furthermore, HDL also carries sphingosine-1-phosphate (S1P),[15] a potent anti-apoptotic sphingolipid, which may contribute to the anti-apoptotic capabilities of HDL.[16] Finally, HDL also carries miRNAs, such as miR-126 and miR92a[21] which are involved in vascular biology and inflammation, and miR-223, which regulates SR-B1 expression.[22] The importance of these different processes and their relative contribution to the prevention of cardiovascular disease remains unknown.

Through high-resolution microscopy and fluorescently labelled lipoproteins, the results from this study propose a mechanism by which HDL directly slows cardiovascular development, preventing LDL transcytosis and deposition in the aorta via competitive associations with SR-B1. Importantly, HDL-mediated inhibition of LDL internalization and transcytosis was observed at physiological concentrations of HDL_2 compared to previous studies which examined non-physiological excess amounts of HDL.[3,48] Together this suggests that physiological HDL, in particular HDL_2, may also partially inhibit SR-B1-mediated LDL transit into the intimal space and thus impede the development of atherosclerosis.

SR-B1 is established as the canonical HDL receptor as excess HDL can effectively compete with LDL binding SR-B1 while excess LDL can only partially compete with HDL for SR-B1 binding.[48,49] Furthermore, the ability of HDL to inhibit LDL transcytosis was hinted at in a previous study in our lab using 25- to 50-fold excess unlabelled HDL by protein mass (relative to LDL).[3,48] Our current study examined lower excess levels of $rHDL^{ApoA1}$and our findings indicate that $rHDL^{ApoA1}$ is able to inhibit LDL internalization and transcytosis at as little as 1x fold excess of $rHDL^{ApoA1}$ compared to LDL. This concentration represents physiological relevant amounts of HDL to LDL. Additionally, the $rHDL^{ApoA1}$ used here was HDL_2-like in density, which is reported to be the preferred substrate of SR-B1 (as monitored by binding or efflux). This $rHDL^{ApoA1}$ was a better inhibitor of LDL uptake and transcytosis than free-ApoA1 (**Figure 3B & 5C**).

Carriers of the Milano mutation have low levels of plasma HDL and elevated triglycerides but do not present any features of HDL deficiency disorders and show no evidence of cholesterol deposition in tissues or atherosclerotic vascular diseases.[33,36] Understanding the mechanistic changes that explain why Milano carriers have low ApoA1 levels yet are resistant to CAD has been elusive. The ApoA1-Milano mutation, Arg 163 to Cys, provides a potential intermolecular disulphide bond formation and dimerization of two ApoA1-Milano proteins. The presence of the disulphide bond locks a proportion of ApoA1-Milano protein in a dimer conformation than ApoA1-WT. Similarly, there may be slight differences in ApoA1-Milano monomers compared to ApoA1-WT monomers. The arginine in ApoA1-WT is involved in forming intrahelical salt bridges with glutamic acid at position 169, this would instead be replaced by repulsion from the cysteine residue in the Milano mutation.[50] As shown by mutation studies, this results in ApoA1-Milano being less stable and having more exposed hydrophobic regions than ApoA1-WT.[50] Other studies sought to determine the secondary structure of ApoA1-Milano and have led to conflicting conclusions where some observed increases in alpha-helical content,[51,52]. In contrast, others observed decreases[50,53] or no change compared to ApoA1-WT.[54]

Similar to $rHDL^{WT}$, $rHDL^{Mil}$ also had a superior ability to inhibit LDL uptake compared to the free ApoA1-Milano (**Figure3B, 4B**). This suggests that the interaction of each to SR-B1 was similar and that the arrangement of ApoA1-Milano and ApoA1-WT in an HDL particle are similar. Indeed, the structure of wild-type and Milano ApoA1 within HDL is thought to be similar based on crosslinking and mass-spectrometry studies.[55,56]Further structural studies of ApoA1-Milano (full length or truncations) through X-ray crystallography or NMR would provide more insight into potential structural differences between wild-type and Milano ApoA1. Cardiovascular disease remains a health problem without a cure due to the complexity of the lipoprotein family, especially HDL. Considering the observation that SR-B1- mediated LDL transcytosis contributes to the formation of atherosclerosis, we propose that an additional way ApoA1 and HDL are beneficial is by continuous competitive binding to SR-B1, thereby impairing LDL transit into the intimal space and slowing the development of atherosclerosis. We observed that excess ApoA1 protein could slightly impede LDL internalization, while physiological relevant levels (relative to LDL) of lipid-associated ApoA1 in reconstituted HDL were sufficient to inhibit LDL internalization partially. This inhibitory property of ApoA1 is only

observable in experiments involving extended incubation periods (*in vitro* LDL uptake and *in vivo* LDL transcytosis assay compared to *in vitro* LDL transcytosis assay), which supports our hypothesis. Furthermore, ApoA1-Milano was a better inhibitor of LDL internalization than ApoA1-WT in its lipid-free form but was a comparable inhibitor to ApoA1-WT in its lipid-associated form in reconstituted HDL. These findings reiterate that ApoA1 is required for the interaction between HDL and SR-B1 and the importance of ApoA1 modifications (such as the lipidation state and the Milano mutation) on its association with SR-B1 to inhibit LDL internalization.

Acknowledgments: The authors would like to thank the Kennan Research Center for Biomedical Science Core Facilities at St. Michael's Hospital, especially Dr. Caterina Di Ciano-Oliveira and Dr. Monika Lodyga, for their continued support, technical advice, expertise and training.

Funding: This work was supported by the Canadian Consortium on Neurodegeneration in Aging (CCNA) and an Natural Sciences and Engineering Research Council (NSERC) of Canada Discovery Grant (RPGIN-2019-04425) to GDF. GDF is also supported by a Tier 1 Canada Research Chair in Multiomics of Lipids and Innate Immunity. WLL is supported by a Canada Research Chair in Mechanisms of Endothelial Permeability and operating funds from a CHRP grant (CPG 158284; CHRP 523598) from the CIHR/NSERC.

Competing interests: The authors declare no competing interests.

Data and materials availability: All data is available in the main text or supplementary materials.

References

1. Gimbrone, M. A. & García-Cardeña, G. Vascular endothelium, hemodynamics, and the pathobiology of atherosclerosis. *Cardiovasc. Pathol.* **22**, 9–15 (2013).

2. Moore, K. J., Sheedy, F. J. & Fisher, E. A. Macrophages in atherosclerosis: A dynamic balance. *Nat. Rev. Immunol.* **13**, 709–721 (2013).

3. Armstrong, S. M. *et al.* A novel assay uncovers an unexpected role for SR-BI in LDL transcytosis. *Cardiovasc. Res.* **108**, 268–277 (2015).

4. Huang, L. *et al.* SR-B1 drives endothelial cell LDL transcytosis via DOCK4 to promote atherosclerosis. *Nature* (2019). doi:10.1038/s41586-019-1140-4

5. Kraehling, J. R. *et al.* Genome-wide RNAi screen reveals ALK1 mediates LDL uptake and transcytosis in endothelial cells. *Nat. Commun.* **7**, (2016).

6. Rohrer, L. *et al.* High-density lipoprotein transport through aortic endothelial cells involves scavenger receptor BI and ATP-binding cassette transporter G1. *Circ. Res.* **104**, 1142–1150 (2009).

7. Randolph, G. J. & Miller, N. E. Lymphatic transport of high-density lipoproteins and chylomicrons. *J. Clin. Invest.* **124**, 929–35 (2014).

8. Baker, P. W., Rye, K. A., Gamble, J. R., Vadas, M. A. & Barter, P. J. Ability of reconstituted high density lipoproteins to inhibit cytokine- induced expression of vascular cell adhesion molecule-1 in human umbilical vein endothelial cells. *J. Lipid Res.* **40**, 345–353 (1999).

9. Calabresi, L. *et al.* Inhibition of VCAM-1 expression in endothelial cells by reconstituted high density lipoproteins. *Biochem. Biophys. Res. Commun.* **238**, 61–65 (1997).

10. Cockerill, G. W., Rye, K. A., Gamble, J. R., Vadas, M. A. & Barter, P. J. High-density lipoproteins inhibit cytokine-induced expression of endothelial cell adhesion molecules. *Arter. Thromb Vasc Biol* **15**, 1987–1994 (1995).

11. Van Lenten, B. J., Navab, M., Shih, D., Fogelman, A. M. & Lusis, A. J. The role of high-density lipoproteins in oxidation and inflammation. *Trends Cardiovasc. Med.* **11**, 155–161 (2001).

12. Navab, M. *et al.* The oxidation hypothesis of atherogenesis: The role of oxidized phospholipids and HDL. *J. Lipid Res.* **45**, 993–1007 (2004).

13. Shih, D. M. *et al.* Mice lacking serum paraoxonase are susceptible to organophosphate toxicity and atherosclerosis. *Nature* **394**, 284–287 (1998).

14. Tward, A. *et al.* Decreased atherosclerotic lesion formation in human serum paraoxonase transgenic mice. *Circulation* **106**, 484–490 (2002).

15. Nofer, J. R. *et al.* HDL induces NO-dependent vasorelaxation via the lysophospholipid receptor S1P3. *J. Clin. Invest.* **113**, 569–581 (2004).

16. Kimura, T. *et al.* Sphingosine 1-Phosphate May Be a Major Component of Plasma Lipoproteins Responsible for the Cytoprotective Actions in Human Umbilical Vein Endothelial Cells *. *J. Biol. Chem.* **276**, 31780–31785 (2001).

17. Robbesyn, F. *et al.* HDL counterbalance the proinflammatory effect of oxidized LDL by inhibiting intracellular reactive oxygen species rise, proteasome activation, and subsequent NF-?B activation in smooth muscle cells. *FASEB J.* **17**, 743–45 (2003).

18. Suc, I. *et al.* HDL and ApoA Prevent Cell Death of Endothelial Cells Induced by Oxidized LDL. *Arter. Thromb Vasc Biol* **17**, 2158–2166 (1997).

19. Seetharam, D. High-Density Lipoprotein Promotes Endothelial Cell Migration and Reendothelialization via Scavenger Receptor-B Type I. *Circ. Res.* **98**, 63–72 (2005).

20. Norata, G. D., Callegari, E., Inoue, H. & Catapano, A. L. HDL3 Induces Cyclooxygenase-2 Expression and Prostacyclin Release in Human Endothelial Cells Via a p38 MAPK/CRE-Dependent Pathway: Effects on COX-2/PGI-Synthase Coupling. *Arterioscler. Thromb. Vasc. Biol.* **24**, 871–877 (2004).

21. Wagner, J. *et al.* Clinical and Population Studies Characterization of Levels and Cellular Transfer of Circulating Lipoprotein-bound MicroRNAs. *Arter. Thromb Vasc Biol* **33**, 1392–1400 (2013).

22. Vickers, K. C., Palmisano, B. T., Shoucri, B. M., Shamburek, R. D. & Remaley, A. T. MicroRNAs are Transported in Plasma and Delivered to Recipient Cells by High-Density Lipoproteins. *Nat. Cell Biol.* **13**, 423–433 (2011).

23. Fung, K. Y. *et al.* SR-BI Mediated Transcytosis of HDL in Brain Microvascular Endothelial Cells Is Independent of Caveolin, Clathrin, and PDZK1. *Front. Physiol.* **8**, 841 (2017).

24. Zhang, Y. *et al.* Overexpression of Apolipoprotein A-I Promotes Reverse Transport of Cholesterol From Macrophages to Feces In Vivo. *Circulation* 1–4 (2003). doi:10.1161/01.CIR.0000086981.09834.E0

25. Puranik, R. *et al.* Low dose apolipoprotein A-I rescues carotid arteries from inflammation in vivo. *Atherosclerosis* **196**, 240–247 (2008).

26. Garner, B., Waldeck, A. R., Witting, P. K., Rye, K. A. & Stocker, R. Oxidation of high density lipoproteins. II. Evidence for direct reduction of lipid hydroperoxides by methionine residues of apolipoproteins AI and AII. *J. Biol. Chem.* **273**, 6088–95 (1998).

27. Garner, B. *et al.* Oxidation of high density lipoproteins. I. Formation of methionine sulfoxide in apolipoproteins AI and AII is an early event that accompanies lipid peroxidation and can be enhanced by alpha-tocopherol. *J. Biol. Chem.* **273**, 6080–7 (1998).

28. Segrest, J. P. *et al.* The amphipathic helix in the exchangeable apolipoproteins: A review of secondary structure and function. *J. Lipid Res.* **33**, 141–166 (1992).

29. Rye, K. & Barter, P. J. Formation and Metabolism of Prebeta-Migrating, Lipid-Poor Apolipoprotein A-I. *Arter. Thromb Vasc Biol* **24**, 421–428 (2004).

30. Borja, M. S. *et al.* HDL-apoA-I Exchange□: Rapid Detection and Association with Atherosclerosis. **8**, (2013).

31. Santos, R. D. *et al.* Clinical presentation, laboratory values, and coronary heart disease risk in marked high-density lipoprotein-deficiency states. *J. Clin. Lipidol.* **2**, 237–247 (2008).

32. Schaefer, E. J., Santos, R. D. & Asztalos, B. F. Marked HDL deficiency and premature coronary heart disease Ernst. *Curr. Opin. Lipidol.* **21**, 289–297 (2010).

33. Weisgraber, K. H. *et al.* A-I Milano Apoprotein. *J. Clin. Invest.* **66**, 901–907 (1980).

34. Franceschini, G., Frosi, T. G., Cristina, M., Gianfranceschi, G. & Sirtori, C. R. High Density Lipoprotein-3 Heterogeneity in Subjects with the ApoAIMilano Variant. *J. Biol. Chem.* **257**, 9926–9930 (1982).

35. Favari, E. *et al.* A unique protease-sensitive high density lipoprotein particle containing the apolipoprotein A-IMilano dimer effectively promotes ATP-binding cassette A1-mediated cell cholesterol efflux. *J. Biol. Chem.* **282**, 5125–5132 (2007).

36. Gualandri, V. *et al.* AIMilano apoprotein identification of the complete kindred and evidence of a dominant genetic transmission. *Am. J. Hum. Genet.* **37**, 1083–97 (1985).

37. Li, Z., Michael, I. P., Zhou, D., Nagy, A. & Rini, J. M. Simple piggyBac transposon-based mammalian cell expression system for inducible protein production. *Proc. Natl. Acad. Sci. U. S. A.* **110**, 5004–9 (2013).

38. Kook, S. *et al.* Impaired Lysosomal Integral Membrane Protein 2-dependent Peroxiredoxin 6 Delivery to Lamellar Bodies Accounts for Altered Alveolar Phospholipid Content in Adaptor Protein-3-deficient pearl Mice. *J. Biol. Chem.* **291**, 8414–27 (2016).

39. Tall, A. R., Small, D. M., Deckelbaum, R. J. & Shipley, G. G. Structure and thermodynamic properties of high density lipoprotein recombinants. *J. Biol. Chem.* **252**, 4701–4711 (1977).

40. Williams, D. L. *et al.* Binding and cross-linking studies show that scavenger receptor BI interacts with multiple sites in apolipoprotein A-I and identify the class A amphipathic α-

helix as a recognition motif. *J. Biol. Chem.* **275**, 18897–18904 (2000).

41. Rothbauer, U. *et al.* A Versatile Nanotrap for Biochemical and Functional Studies with Fluorescent Fusion Proteins. *Mol. Cell. Proteomics* **7**, 282–289 (2008).

42. Azizi, P. M. *et al.* Clathrin-dependent entry and vesicle-mediated exocytosis define insulin transcytosis across microvascular endothelial cells. *Mol. Biol. Cell* **26**, 740–750 (2015).

43. Ghaffari, S., Nabi, F. N., Sugiyama, M. G. & Lee, W. L. Estrogen inhibits LDL (low-density lipoprotein) transcytosis by human coronary artery endothelial cells via GPER (G-protein-coupled estrogen receptor) and SR-BI (scavenger receptor class B type 1). *Arterioscler. Thromb. Vasc. Biol.* **38**, 2283–2294 (2018).

44. Ghaffari, S. *et al.* Endothelial HMGB1 Is a Critical Regulator of LDL Transcytosis via an SREBP2-SR-BI Axis. *Arterioscler. Thromb. Vasc. Biol.* 200–216 (2020). doi:10.1161/ATVBAHA.120.314557

45. De Beer, M. C. *et al.* Apolipoprotein AI conformation markedly influences HDL interaction with scavenger receptor BI. *J. Lipid Res.* **42**, 309–313 (2001).

46. Marques, P. E. *et al.* Multimerization and Retention of the Scavenger Receptor SR-B1 in the Plasma Membrane. *Dev. Cell* **50**, 283-295.e5 (2019).

47. Jerabek-Willemsen, M. *et al.* MicroScale Thermophoresis: Interaction analysis and beyond. *J. Mol. Struct.* **1077**, 101–113 (2014).

48. Angel, A., D'Costa, M. A. & Yuen, R. Low density iboprotein binding, internalizafion, and degradation in human adipose cells. *Can. J. Biochem.* **57**, 578–587 (1979).

49. Acton, S. *et al.* Identification of Scavenger Receptor SR-BI as a High Density Lipoprotein Receptor. *Science (80-.).* **271**, 18–20 (1996).

50. Alexander, E. T. *et al.* Structural and functional consequences of the Milano mutation (R173C) in human apolipoprotein A-I. *J. Lipid Res.* **50**, 1409–1419 (2009).

51. Calabresi, L. *et al.* Molecular characterization of native and recombinant apolipoprotein A- I(Milano) dimer. The introduction of an interchain disulfide bridge remarkably alters the physicochemical properties of apolipoprotein A-I. *J. Biol. Chem.* **269**, 32168–32174 (1994).

52. Petrlova, J. *et al.* Secondary structure changes in ApoA-I Milano (R173C) are not accompanied by a decrease in protein stability or solubility. *PLoS One* **9**, 1–6 (2014).

53. Franceschini, G., Vecchio, G. & Gianfranceschi, G. Apolipoprotein AI(Milano). Accelerated binding and dissociation from lipids of a human apolipoprotein variant. *J. Biol. Chem.* **260**, 16321–16325 (1985).

54. Zhu, X., Wu, G., Zeng, W., Xue, H. & Chen, B. Cysteine mutants of human

apolipoprotein A-I: A study of secondary structural and functional properties. *J. Lipid Res.* **46**, 1303–1311 (2005).

55. Bhat, S., Sorci-Thomas, M. G., Calabresi, L., Samuel, M. P. & Thomas, M. J. Conformation of dimeric apolipoprotein A-I milano on recombinant lipoprotein particles. *Biochemistry* **49**, 5213–5224 (2010).

56. Gursky, O., Jones, M. K., Mei, X., Segrest, J. P. & Atkinson, D. Structural basis for distinct functions of the naturally occurring Cys mutants of human apolipoprotein A-I. *J. Lipid Res.* **54**, 3244–3257 (2013).

Figures

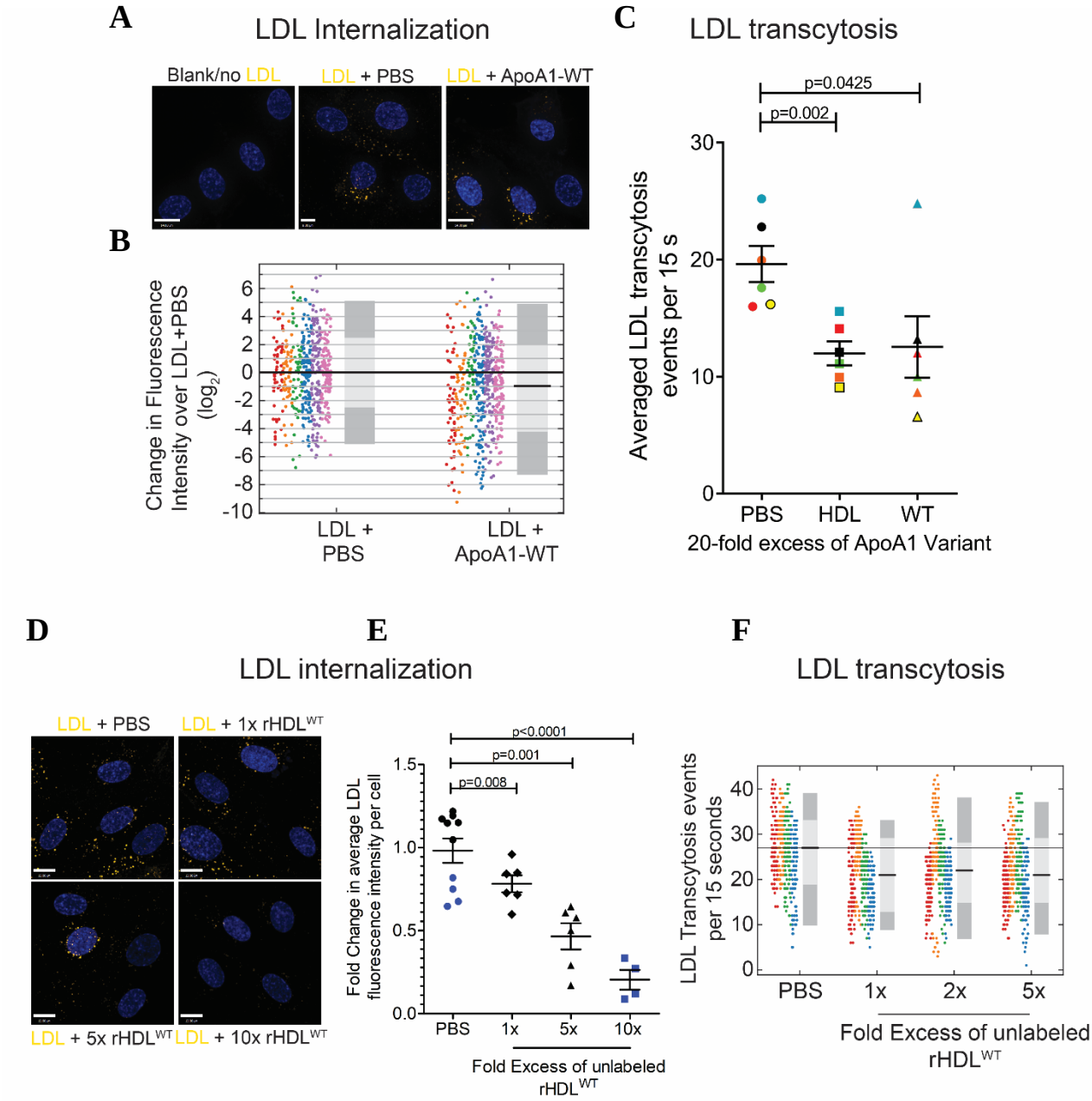

Figure 1. Unlabeled ApoA1/reconstituted HDL inhibits DiI-LDL transcytosis in human coronary endothelial cells. (A) Representative images of internalized DiI-LDL in HCAECs treated with 20-fold excess unlabeled ApoA1-WT. **(B)** Quantification of fold change in DiI-LDL signal per cell normalized to the PBS control (DiI-LDL alone) along with median fold change presented as the black bar and the 95% (dark grey) and 68% (light grey) confidence interval.

Replicates are color coded, n = 6 repetition, where at least 40 cells were quantified per condition per repetition. **(C)** Inhibition of DiI-LDL transcytosis by excess unlabeled ApoA1-WT as measured using TIRF microscopy. Presented are the average transcytosis events over a span of 15 secs per field of view after subtraction from a no DiI-LDL coverslip over n = 6 repetitions. Replicates are color coded, where 10 cells were imaged per condition per repetition. **(D)** Representative images of DiI-LDL internalization competition by 10-, 5-, 1- fold excess of $rHDL^{WT}$ relative to DiI-LDL by protein mass. (**E**) Quantification of the amount of DiI-LDL uptake expressed as fold change compared to DiI-LDL added alone. Replicates are color coded, n=5 for 1x & 5x and n=4 for 10x, where 60 cells were imaged and analyzed per condition per n. (**F**) Inhibition of DiI-LDL transcytosis by excess unlabeled $rHDL^{WT}$ as measured using TIRF microscopy. Presented are the transcytosis events per cell over a span of 15 secs per field of view after subtraction from a no DiI-LDL coverslip along with average fold change presented as the black bar and the 95% (dark grey) and 68% (light grey) confidence interval. Replicates are color coded, n=6, where 10 cells were imaged per condition per n.

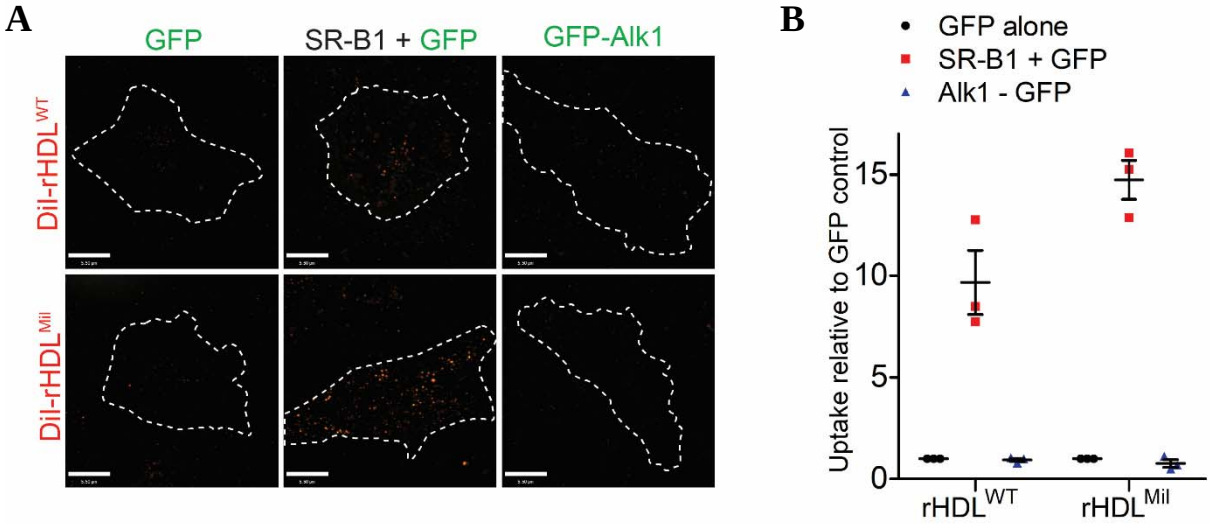
A
GFP
SR-B1 + GFP
GFP-Alk1
DiI-rHDL WT
DiI-rHDL Mil
B
GFP alone
SR-B1 + GFP
Alk1 - GFP
Uptake relative to GFP control
0
5
10
15
rHDL WT
rHDL Mil

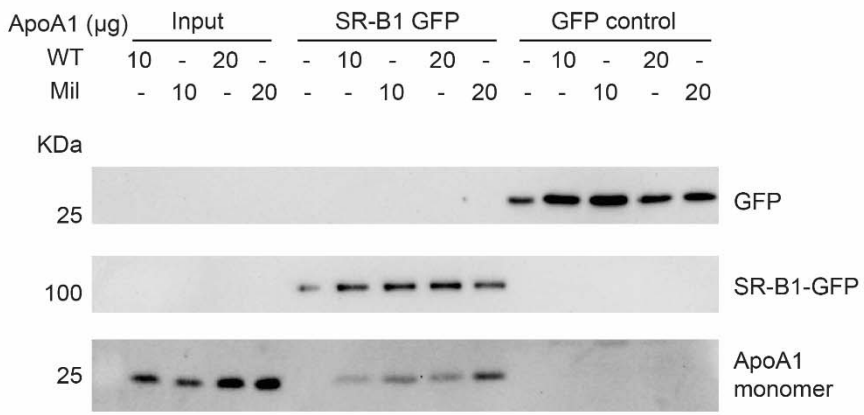
C
ApoA1 (µg)
Input
SR-B1 GFP
GFP control
WT 10 - 20 - - 10 - 20 - - 10 - 20 -
Mil - 10 - 20 - - 10 - 20 - - 10 - 20
KDa
25
GFP
100
SR-B1-GFP
25
ApoA1 monomer

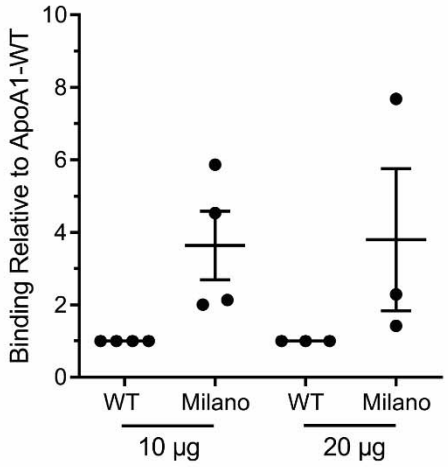
D
Binding Relative to ApoA1-WT
0
2
4
6
8
10
WT
Milano
WT
Milano
10 µg
20 µg

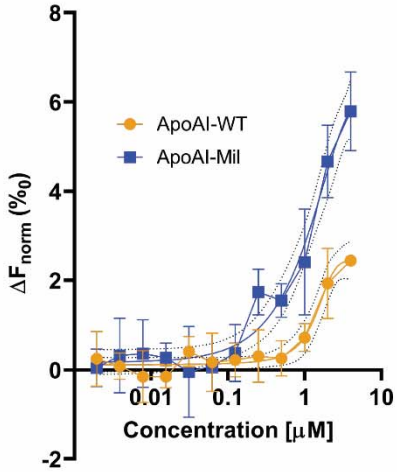
E
ApoAI-WT
ApoAI-Mil
ΔFnorm (‰)
-2
0
2
4
6
8
0.01
0.1
1
10
Concentration [µM]

Figure 2. ApoA1/reconstituted HDL interacts with SR-B1 while ApoA1-Milano shows enhance binding to SR-B1 compared to ApoA1-WT. (A) Representative images of rHDL^{WT} or rHDL^{Mil} incubated with HeLa cells transiently overexpressing SR-B1 + GFP, GFP-Alk1 and the control GFP alone. **(B)** The amount of rHDL^{WT} or rHDL^{Mil} signal per cell was averaged and normalized to the basal amount seen when transfected with GFP alone. n=3 for either experiments where 15 cells were imaged and analyzed per condition per n. **(C)** Representative western blot of the ApoA1-SRB1-GFP binding assay along with the quantification **(D)** expressed as fold change compared to ApoA1-WT interaction with SR-B1-GFP that has been normalized to ApoA1 in the input and amount of SR-B1 immobilized. n=6 for 10ug ApoA1; n=5 for 20ug ApoA1. **(E)** Binding of various concentrations of ApoA1-WT or ApoA1-Mil to 50nM SR-B1 as measured by microscale thermophoresis.

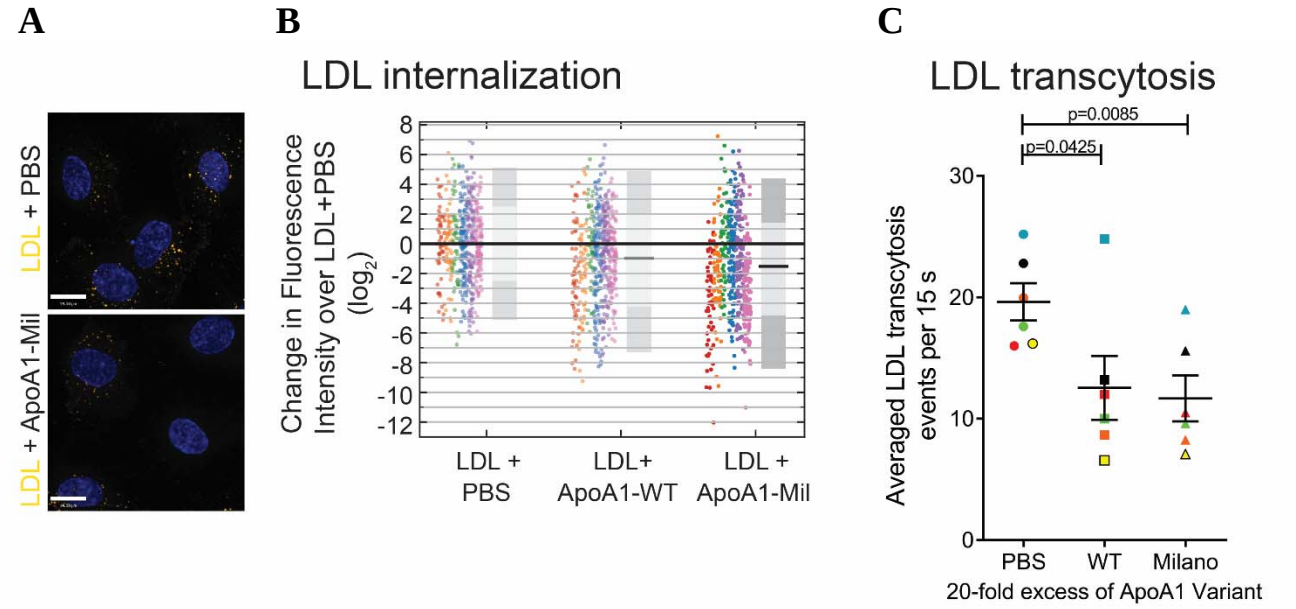

Figure 3. Recombinant ApoA1-Milano inhibit DiI-LDL internalization and transcytosis in human coronary endothelial cells. (A) Representative images and the quantification of the affect of adding excess unlabeled ApoA1-Milano on internalization of DiI-LDL in coronary endothelial cells. **(B)** Quantification of fold change in DiI-LDL signal per cell normalized to the PBS control (DiI-LDL alone) along with median fold change presented as the black bar and the 95% (dark grey) and 68% (light grey) confidence interval. Replicates are color coded, n = 6 repetition, where at least 40 cells were quantified per condition per repetition. **(C)** Inhibition of DiI-LDL transcytosis by excess unlabeled ApoA1-Mil as measured using TIRF microscopy. Presented are the average transcytosis events over a span of 15 secs per field of view after

subtraction from a no DiI-LDL coverslip n=6. Replicates are color coded, where 10 cells were imaged per condition per n.

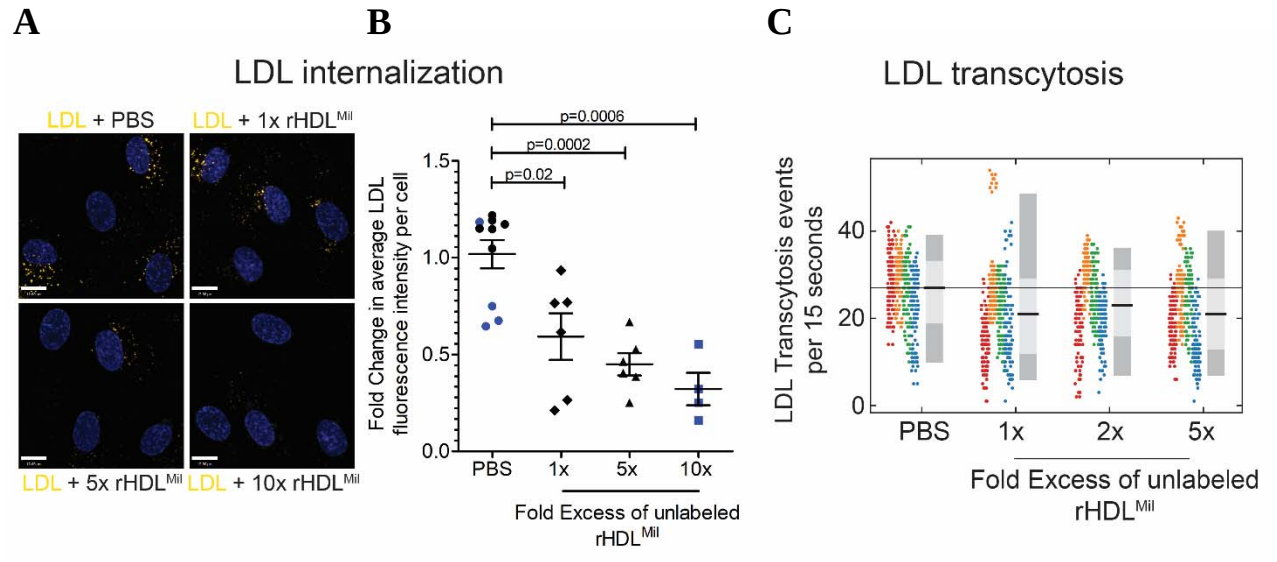

Figure 4. Inhibition of DiI-LDL internalization and transcytosis using physiological doses of unlabeled rHDL^{Mil} in human coronary endothelial cells. (A) Representative images of DiI-LDL internalization competition by 10-, 5-, 1- fold excess of rHDL^{Mil} relative to DiI-LDL by protein mass. **(B)** Quantification of the amount of DiI-LDL uptake expressed as fold change compared to DiI-LDL added alone. Replicates are color coded, n=5 for 1x & 5x and n=4 for 10x, where 60 cells were imaged and analyzed per condition per n. (**C**) Inhibition of DiI-LDL transcytosis by excess unlabeled rHDL^{Mil} as measured using TIRF microscopy. Presented are the transcytosis events per cell over a span of 15 secs per field of view after subtraction from a no DiI-LDL coverslip along with average fold change presented as the black bar and the 95% (dark grey) and 68% (light grey) confidence interval. Replicates are color coded, n=6, where 10 cells were imaged per condition per n.

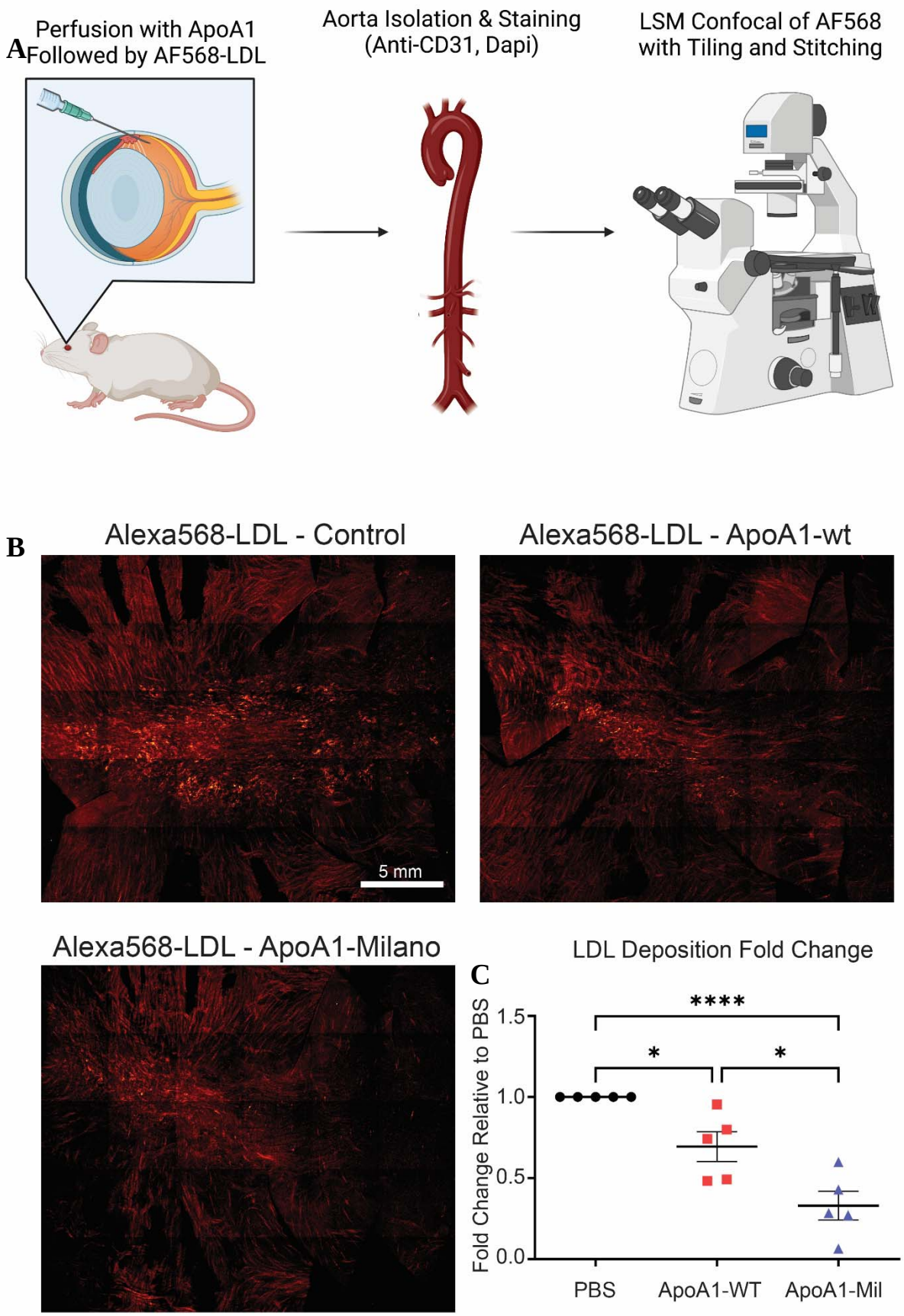
A
Perfusion with ApoA1
Followed by AF568-LDL
Aorta Isolation & Staining
(Anti-CD31, Dapi)
LSM Confocal of AF568
with Tiling and Stitching
B
Alexa568-LDL - Control
Alexa568-LDL - ApoA1-wt
5 mm
Alexa568-LDL - ApoA1-Milano
C
LDL Deposition Fold Change
Fold Change Relative to PBS
1.5
1.0
0.5
0.0
****
*
*
PBS
ApoA1-WT
ApoA1-Mil

Figure 5. Recombinant ApoA1 inhibits deposition of AF568-LDL in mice aorta. (A) Schematic outline of the *in vivo* procedure to measure LDL deposition in mice aorta from treatment to image acquisition of the isolated aorta. **(B)** Representation images of en face staining of the isolated aortas from mice perfused with PBS or 0.4 mg of ApoA1-WT or ApoA1-Milano prior to perfusion with AF568-LDL (red) through retro-orbital injection. **(C)** Quantification of LDL fluorescence from en face staining of the isolated aortas, values are normalized to basal AF568-LDL deposition in PBS perfused mice. n=5, * $p<0.05$, **** $p<0.0001$.

Supplemental Figures

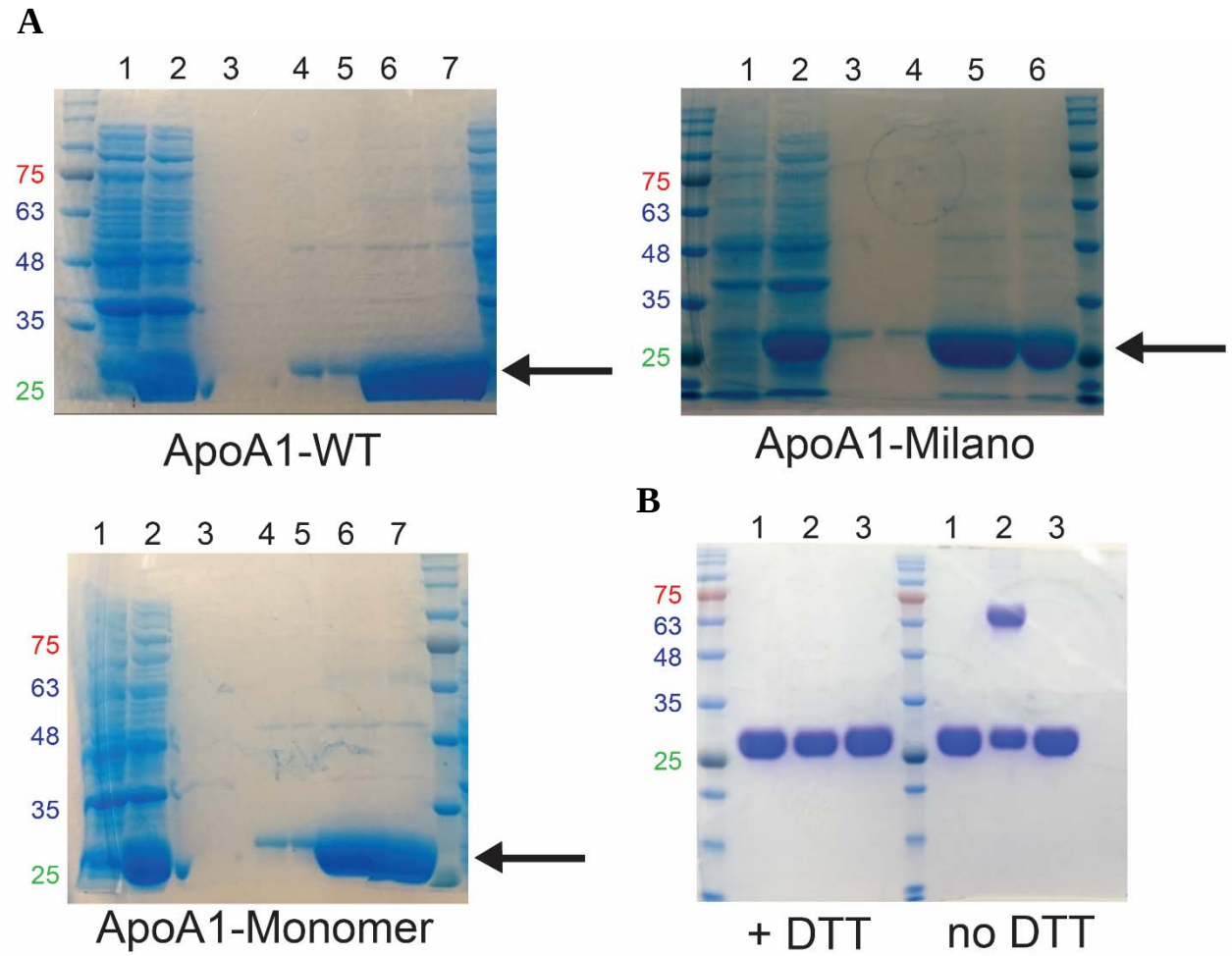

Supplemental Figure 1. SDS PAGE analysis of the purification of the ApoA1 variants. (A) The resulting SDS PAGE gel looking at the purification process of the three ApoA1 variants where the arrow indicates the ApoA1 protein. The loading order is of the following: for ApoA1-WT and ApoA1-Monomer, 1) Not Induced, soluble 2) 1 mM IPTG induced, soluble, 3) Flow thru from purification, 4) Wash 4 (10 mM Imidazole), 5) Wash 5 (10 mM Imidazole), 6) Elution with 0.1 M EDTA, 7) Dialyzed Elution (in PBS). For ApoA1-Mil: 1) Not Induced, soluble 2) 1 mM IPTG induced, soluble, 3) Wash 4 (10 mM Imidazole), 4) Wash 5 (10 mM Imidazole), 5) Elution with 0.1 M EDTA, 6) Dialyzed Elution (in PBS). **(B)** The resulting SDS PAGE gel of sample treated with out without DTT to assess the disulfide bond state of ApoA1-Mil. The loading order is of the following: 1) ApoA1-WT 2) ApoA1-Mil 3) ApoA1-Monomer.

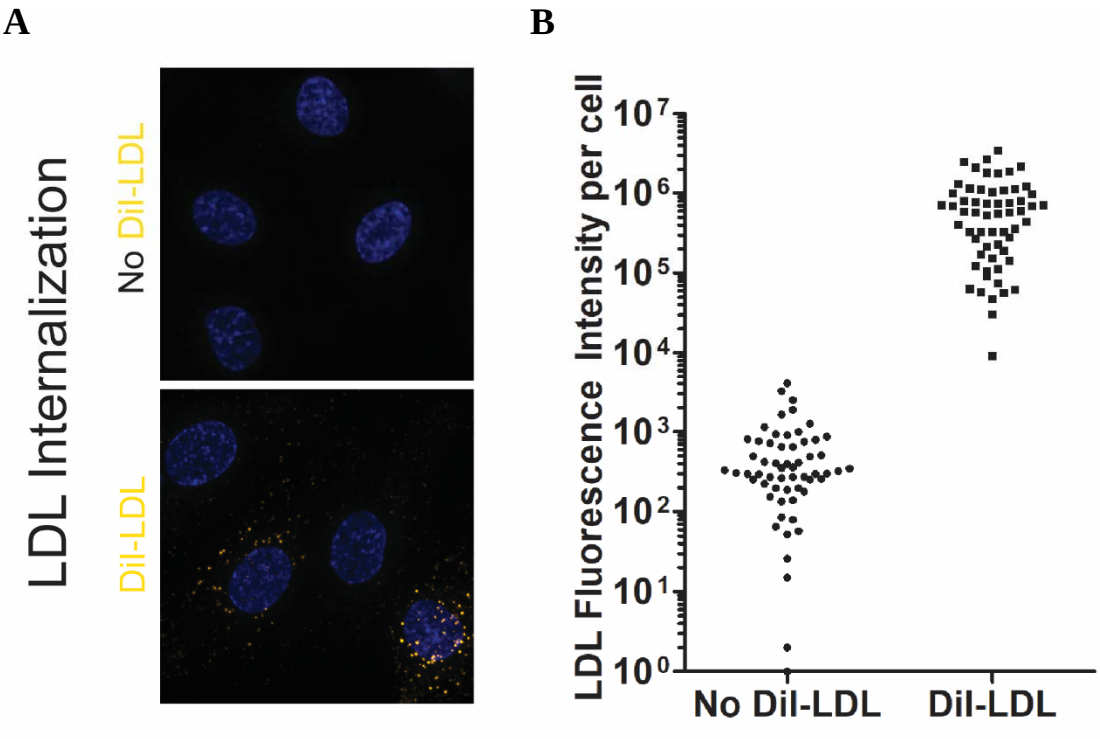

Supplemental Figure 2. Heterogeneity in the amount of DiI-LDL internalized in human coronary endothelial cells as measured through DiI fluorescence per cell. (A) Representative image of DiI-LDL internalization in HCAECs accompanied with **(B)** quantification of the integrated density of DiI-LDL fluorescence per cell of a typical replicate experiment.

A

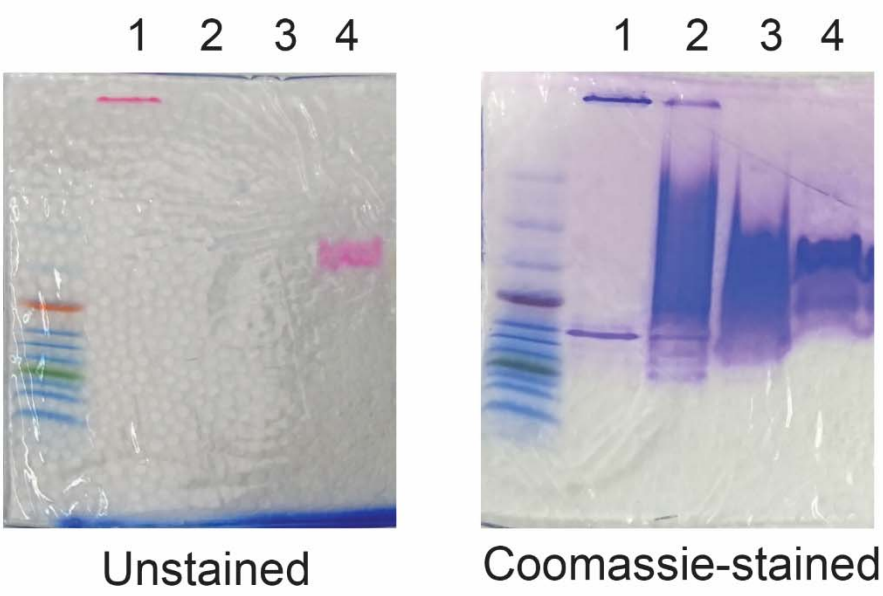

B

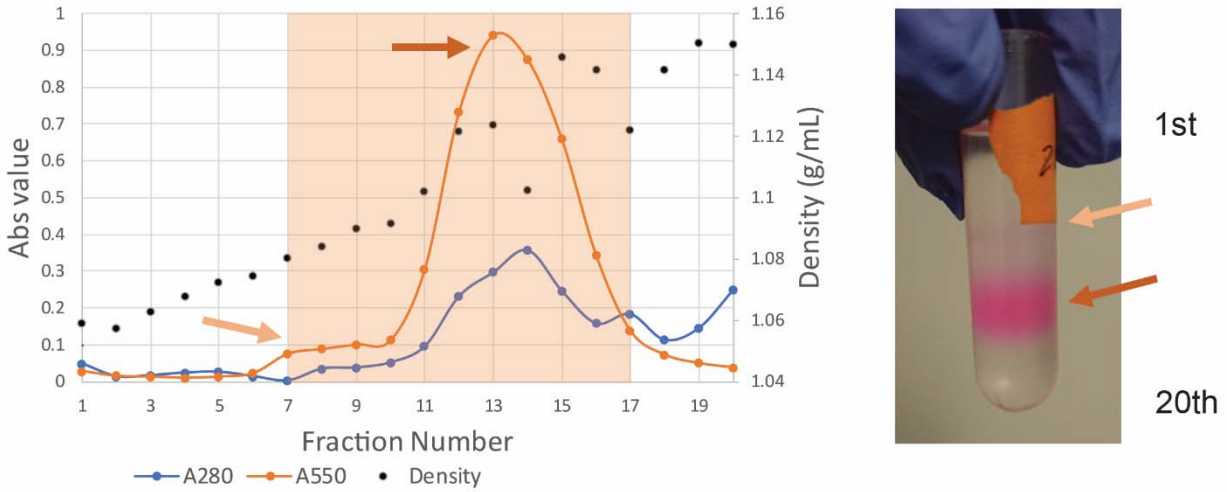

Supplemental Figure 3. Assessing the generated rHDL^{ApoA1} particles. (A) Native gel analysis to gauge the size of the generated DiI- rHDL^{ApoA1} (lane 4) made from recombinant ApoA1 (lane 3) in comparison to isolated DiI-LDL (lane 1) and commercially purchased HDL (lane 2). The gel was generated with made with polyacrylamide and the system ran at pH 8.75. **(B)** Plot of the density of the generated DiI-DMPC-WT particles measured manually along with absorbances at 280 nm and 555 nm to detect ApoA1-WT and DiI respectively).

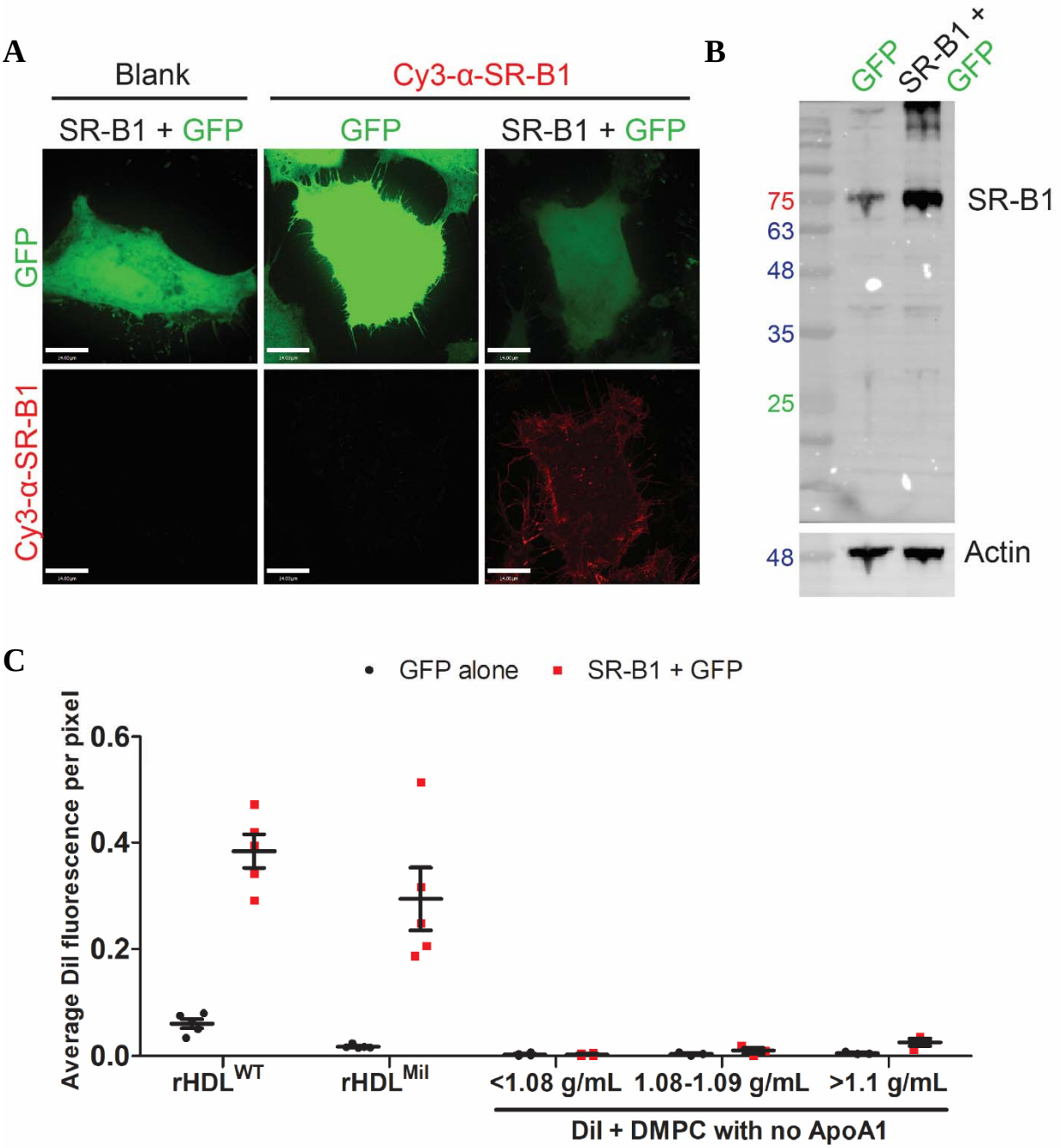

Supplemental Figure 4. Verifying bi-cistronic SR-B1 + GFP plasmid through IF and western blot and association specific association with ApoA1 containing particles. (A) Representative images of HeLa cells transfected with GFP alone or the bi-cistronic SR-B1 + GFP plasmid stained with a Cy3-conjugated SR-B1 nanobody. **(B)** Lysate collected from HeLa cells transfected with GFP alone or the bi-cistronic SR-B1 + GFP plasmid ran on a western blot

and was probed with an SR-B1 antibody to verify that full length SR-B1 was overexpressed compared to the GFP-alone transfected HeLa cells. **(C)** Quantification of uptake of different densities (all of which span the density of natural HDL) of DMPC and DiI particles that lack ApoA1 by SR-B1 + GFP and GFP overexpressing HeLa cells. n=4 for <1.08 g/mL, n=3 for 1.08-1.09 g/mL and for >1.1 g/mL, where 15 cells were imaged and analyzed per condition per n.